Protein kinase Cα gain-of-function variant in Alzheimer's disease displays enhanced catalysis by a mechanism that evades down-regulation

Julia A. Callender[a,b], Yimin Yang[a], Gema Lordén[a], Natalie L. Stephenson[c], Alexander C. Jones[b], John Brognard[c,d], and Alexandra C. Newton[a,1]

[a]Department of Pharmacology, University of California, San Diego, La Jolla, CA 92093; [b]Biomedical Sciences Graduate Program, University of California, San Diego, La Jolla, CA 92093; [c]Cancer Research UK Manchester Institute, The University of Manchester, Manchester 4BX M20, United Kingdom; and [d]Laboratory of Cell and Developmental Signaling, National Cancer Institute at Frederick, Frederick, MD 21702

Conventional protein kinase C (PKC) family members are reversibly activated by binding to the second messengers Ca^{2+} and diacylglycerol, events that break autoinhibitory constraints to allow the enzyme to adopt an active, but degradation-sensitive, conformation. Perturbing these autoinhibitory constraints, resulting in protein destabilization, is one of many mechanisms by which PKC function is lost in cancer. Here, we address how a gain-of-function germline mutation in PKCα in Alzheimer's disease (AD) enhances signaling without increasing vulnerability to down-regulation. Biochemical analyses of purified protein demonstrate that this mutation results in an ~30% increase in the catalytic rate of the activated enzyme, with no changes in the concentrations of Ca^{2+} or lipid required for half-maximal activation. Molecular dynamics simulations reveal that this mutation has both localized and allosteric effects, most notably decreasing the dynamics of the C-helix, a key determinant in the catalytic turnover of kinases. Consistent with this mutation not altering autoinhibitory constraints, live-cell imaging studies reveal that the basal signaling output of PKCα-M489V is unchanged. However, the mutant enzyme in cells displays increased sensitivity to an inhibitor that is ineffective toward scaffolded PKC, suggesting the altered dynamics of the kinase domain may influence protein interactions. Finally, we show that phosphorylation of a key PKC substrate, myristoylated alanine-rich C-kinase substrate, is increased in brains of CRISPR-Cas9 genome-edited mice containing the PKCα-M489V mutation. Our results unveil how an AD-associated mutation in PKCα permits enhanced agonist-dependent signaling via a mechanism that evades the cell's homeostatic down-regulation of constitutively active PKCα.

protein kinase C | PKC | Alzheimer's disease | signal transduction | enzyme mutation

Protein kinase C α (PKCα) is a ubiquitously expressed member of the protein kinase C (PKC) family of serine/threonine kinases that transduces signals mediated by the second messengers Ca^{2+} and diacylglycerol (DG) (1, 2). It plays a major role in suppressing cell proliferation (3–7) and survival (8, 9). Studies both in mice, where its deletion causes the spontaneous development of colon tumors (10), and in patients, where loss of protein expression is associated with colon cancer (11), have long supported a role as a tumor suppressor. It is the first PKC in which a cancer-associated mutation was reported: Over 20 y ago, Joubert and coworkers reported that a mutation in PKCα in human pituitary tumors resulted in mislocalization, thus allowing growth in soft agar in ectopic expression studies (12–14). Loss-of-function somatic mutations in PKCα have now been identified in many diverse cancers (15). Mounting evidence suggests that PKCα opposes oncogenic survival signaling by its phosphorylation and inactivation of oncogenes such as K-Ras (8, 16), growth factor receptors (17–19), and phosphatidylinositol-3 kinase (20–22), among others. The key role of PKCα in suppressing proliferative and survival pathways poise it to play a role not only in cancer via its loss of function but also in degenerative diseases via gain of function.

We recently identified gain-of-function mutations in PKCα in Alzheimer's disease (AD) (23), a degenerative pathology characterized by the accumulation of amyloid-β (Aβ) protein aggregates in the brain and synaptic degeneration (24). Whole-genome sequencing of individuals from 410 families with late-onset AD identified germline PKCα mutations in affected, but not in disease-free, individuals in six of the families. These mutations all enhanced the agonist-evoked signaling output of PKCα assessed using a genetically-encoded PKC activity sensor in overexpression studies (23). While the mechanisms by which Aβ aggregation leads to synaptic degeneration are not fully understood, electrophysiological studies established that the synaptic effects of Aβ depend on PKCα via a mechanism requiring PKCα's PDZ ligand [which scaffolds to PDZ domain-containing proteins such as PSD95, SAP97, and PICK1 (25, 26)] and its interaction with the scaffold PICK1 (23, 27). Thus, enhanced activity of PKCα may augment the degenerative pathways activated by Aβ. Supporting a general role of enhanced PKC activity in AD, a recent unbiased phosphoproteomics study identified increased phosphorylation of PKC substrates, including myristoylated alanine-rich C-kinase substrate (MARCKS), as a primary early event in AD (28). These activity-enhancing mutations are in stark contrast to loss-of-function cancer-associated mutations. Indeed, with the possible exception of a mutation in PKCβ in adult T-cell leukemia (29), it is noteworthy

Significance

This work unveils how an Alzheimer's disease-associated mutation (M489V) in protein kinase Cα (PKCα) enhances catalytic activity without sensitizing the protein to the cell's homeostatic degradation of aberrantly active PKCα. The active conformation of wild-type PKC is sensitive to degradation, and therefore constitutively activated PKC paradoxically manifests as loss of function. We show that PKCα-M489V enhances the intrinsic catalytic rate of the kinase without altering the equilibrium between the autoinhibited (protected) conformation and the activated (degradation-sensitive) conformation. Thus, the on/off dynamics are unchanged, but reactions are catalyzed at a faster rate when the enzyme is on. These findings are significant because they provide a mechanism through which a disease mutation in PKCα causes aberrant activation without resulting in paradoxical loss of function via degradation.

BIOCHEMISTRY

that no gain-of-function mutations in any of the nine PKC isozymes have been identified (15).

PKCα is an exquisitely tuned enzyme whose signaling output depends not only on binding to second messengers but also on the abundance of inputs that control its steady-state levels in the cell. Following its biosynthesis, PKCα becomes constitutively phosphorylated at three priming sites, allowing it to adopt an autoinhibited conformation in the cytosol that protects the enzyme from dephosphorylation and degradation (1). Because this autoinhibited species is resistant to degradation, PKCα is a particularly long-lived enzyme. It is transiently and reversibly activated by signals that promote phospholipid hydrolysis to generate its two second messengers, Ca^{2+} and DG: Ca^{2+} binds the C2 domain, promoting association to the plasma membrane via a Ca^{2+}-dependent bridge with anionic phospholipids, and DG binds one of two tandem C1 domains (30). Engagement of both membrane-targeting modules with the plasma membrane results in release of an autoinhibitory pseudosubstrate segment from the substrate-binding cavity, positioning PKC in an "open" and signaling-competent conformation. Metabolism of DG results in PKC disengaging from the membrane and regaining the stable, autoinhibited conformation (30). Phorbol esters, potent competitive ligands for DG binding, are not readily metabolized and therefore result in irreversible binding of PKC to the membrane, leading to acute activation but chronic down-regulation of PKC protein levels (31, 32). The paradoxical effect of these potent tumor promoters—initial activation followed by eventual degradation—confounded understanding the role of PKC in cancer (9). Given that the active conformation of PKC is sensitive to degradation, how do AD-associated mutations result in enhanced cellular kinase activity while also evading down-regulation?

Here, we examine the mechanism by which one AD-associated variant, PKCα-M489V, enhances PKCα signaling. This variant was identified in seven individuals in four families: It is heterozygous, with one allele encoding a protein with a Met-to-Val substitution at position 489 in the activation loop, a segment near the entrance to the active site that critically controls catalysis (33). Our findings support a model in which altered dynamics of the kinase domain enhance the activity of the PKCα-M489V variant by increasing the intrinsic catalytic rate of the enzyme without affecting autoinhibitory constraints. Thus, the enzyme's on/off dynamics are unaffected, but when on it catalyzes phosphorylation at a faster rate. This provides a previously undescribed mechanism by which a disease-associated mutation enhances PKC activity without compromising its stability.

Results

PKCα-M489V Mutation Confers an Enhanced Catalytic Rate. We previously established that PKCα-M489V displays enhanced agonist-evoked signaling output relative to wild-type PKCα in cells (23). Specifically, the M489V variant overexpressed in COS7 cells has ~25% greater activity compared with wild-type enzyme following agonist stimulation of cells to generate Ca^{2+} and DG, as assessed using the genetically-encoded FRET-based C kinase activity reporter (CKAR) (34, 35). This variant has a replacement of Met to Val at position 489 in the activation loop, nine residues before the constitutive phosphorylation site (Thr497) for the upstream kinase PDK-1 (Fig. 1A). It is also two residues removed from an interaction network that connects the activation loop to the C helix, in turn connecting to the C-terminal phosphorylation site Ser657 (Fig. 1C). Furthermore, this face of the kinase domain for the related PKCβII has been shown to interface with the C2 domain to maintain the enzyme in an autoinhibited conformation (36), as
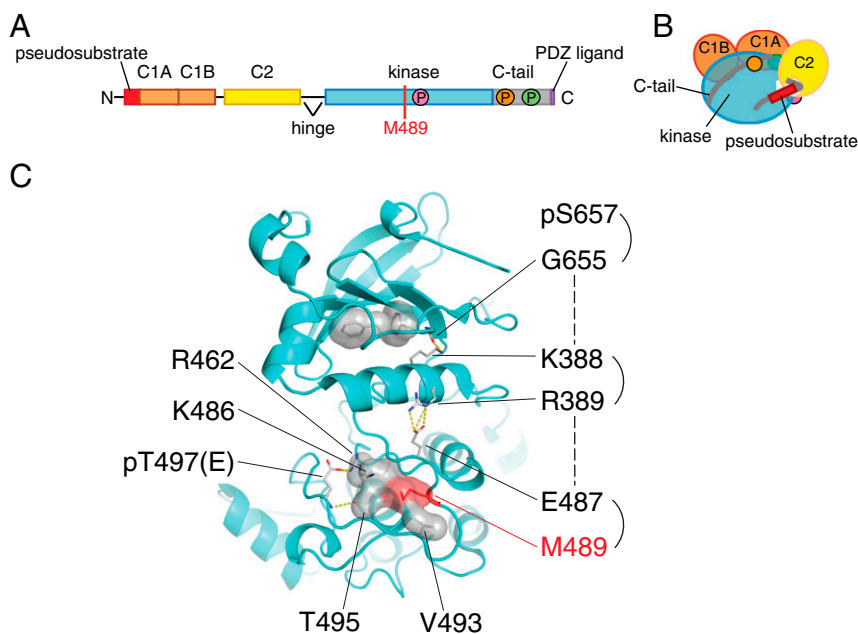

Fig. 1. AD-associated PKCα mutation in key region of catalytic domain. (A) Primary structure of PKCα showing pseudosubstrate (red), C1A and C1B domains (orange), C2 domain (yellow), kinase domain (cyan), C-terminal tail (gray), and PDZ ligand (purple). Indicated are the three processing phosphorylation sites, Thr497 (magenta circle) in the activation loop and Thr638 (orange circle) and Ser657 (green circle) in the C-terminal tail. (B) Cartoon representation showing autoinhibitory constraints in the full-length inactive form of PKCα wherein the pseudosubstrate occupies the substrate binding cavity, an interaction locked in place by the C2 domain. (C) Structure of PKCα kinase domain (PDB ID code 3IW4) showing position of Met489 (red space filling) in the activation loop; note this structure has a Glu at the position of the activation loop phosphorylation site [pT497(E)]. Indicated in stick representation is the network of interactions from the activation loop to the C-terminal tail that involves a salt bridge from Glu487 in the activation loop to Arg389 in the C-helix and H-bonding between the Lys388 in the C-helix to the main chain of Gly655 in the C-terminal tail; H-bonds and salt bridges are indicated by yellow dots. Gly655 is in a conserved FXXF motif that directly precedes the hydrophobic phosphorylation site (phospho-Ser657); the two Phe are indicated in gray space filling model. Residues that pack into the activation loop (Arg462, Lys486, Val493, and Thr495) are also presented in gray space filling model.

schematized in Fig. 1*B*. Thus, this residue is positioned to potentially perturb autoinhibitory constraints, catalysis, or both.

To elucidate the molecular mechanism through which the M489V mutation confers enhanced PKC activity in cells, we analyzed the kinetics of activation of the purified wild-type and M489V mutant protein. GST-tagged PKCα was purified to homogeneity from insect cells using a baculovirus expression system. Western blot analysis confirmed that both the wild-type and PKCα-M489V proteins were processed by priming phosphorylations at the activation loop (Thr497) and the two C-terminal sites (Thr638 and Ser657) (Fig. 2*A*).

To assess whether autoinhibitory constraints were altered in the PKCα-M489V protein, we examined the dependence for activation on (*i*) Ca^{2+} or (*ii*) mole fraction phosphatidylserine (PS) in DG-containing micelles. Triton X-100 lipid mixed micelles afford a highly sensitive system to dissect the lipid dependence of PKC activation, which displays high cooperativity with respect to PS (37–39). Kinase assays revealed no differences in the two proteins with respect to the concentration of Ca^{2+} or PS resulting in half-maximal activity (Fig. 2*B* and Table 1), nor was the basal activity different between the two proteins, which both displayed ~10% of cofactor-induced activity when activators were absent from the assay. We did note, however, that the V_{max} was consistently higher for the PKCα-M489V protein compared with wild-type enzyme. These data reveal that while the autoinhibitory constraints were unaffected in the PKCα-M489V variant, the maximal velocity was higher.

We next assessed whether peptide substrate or ATP dependencies were altered in the AD variant. When assayed in the presence of saturating Ca^{2+} and lipid, the K_m for peptide substrate
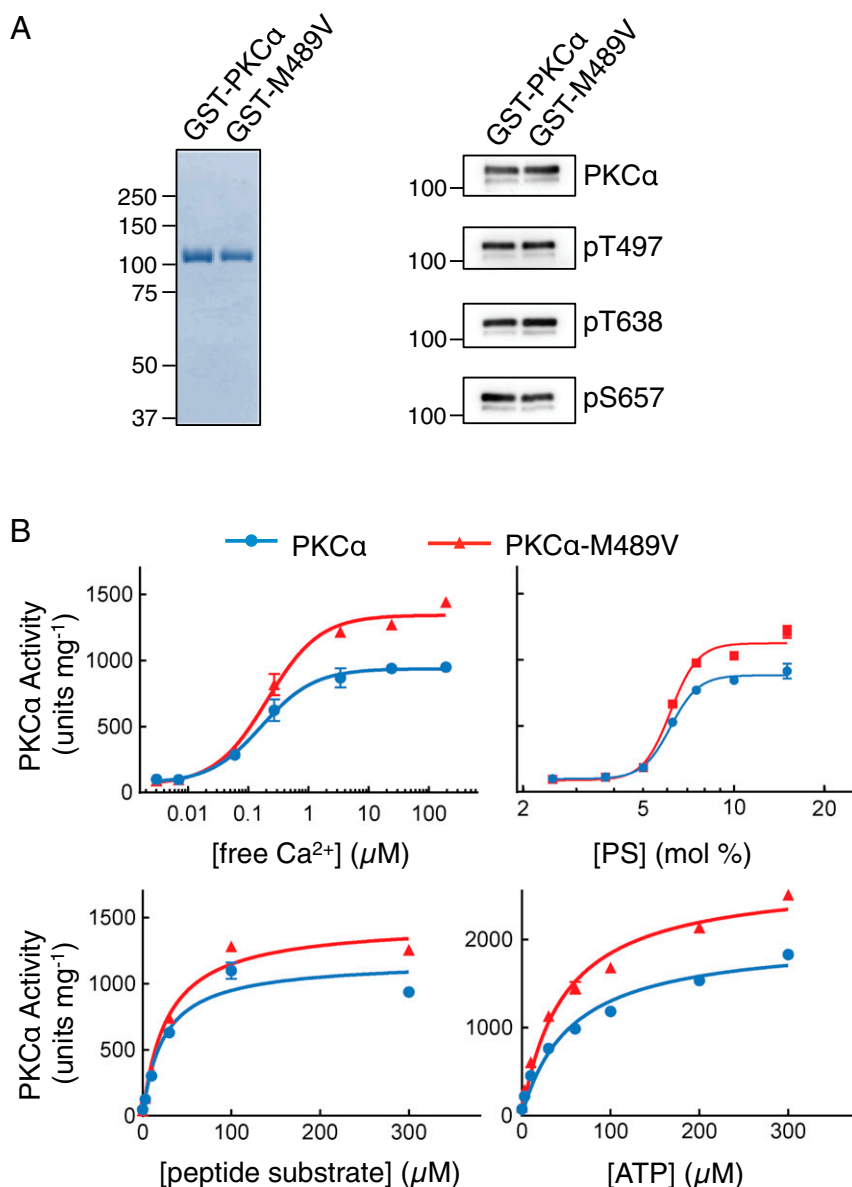

Fig. 2. Purified PKCα-M489V displays higher V_{max} than wild-type PKCα under activating conditions. (*A*) Coomassie Blue-stained SDS/PAGE gel of purified GST-PKCα wild type and GST-PKCα M489V (*Left*). Western blot of pure proteins probed with antibodies for total PKCα, or with phosphospecific antibodies to the priming phosphorylation sites, pT497, pT638, and pS657 (*Right*). (*B*) The activity of PKCα wild type (blue) or M489V (red) (typically 2.4 nM) measured as a function of Ca^{2+}, PS, peptide substrate, or ATP concentration. Data are graphed in units (nanomoles phosphate per minute) per milligram GST-PKC. Data represent the average ± SEM of triplicate samples.

Table 1. Kinetic values for in vitro kinase assays using purified PKCα or PKCα-M489V

Protein	Ca^{2+}_{50}, μM	PS_{50}, mol %	$K_{msubstrate}$, μM	K_{mATP}, μM	V_{max}, units·mg^{-1}
PKCα	0.17 ± 0.05	6.16 ± 0.05	24 ± 5	55 ± 8	$(2.0 \pm 0.2) \times 10^3$
PKCα-M489V	0.21 ± 0.07	6.16 ± 0.06	28 ± 4	47 ± 6	$(2.7 \pm 0.2) \times 10^3$

Kinetic values from the data shown in Fig. 2B are listed. Data represent the average $\pm$ SEM of triplicate samples. Unless otherwise indicated in the figure legends, the standard reaction component concentrations were as follows: 200 μM free Ca^{2+}, Triton X-100 mixed micelles containing 5 mol % DG and 15 mol % phosphatidylserine, 100 μM peptide substrate, and 100 μM ATP. V_{max} is obtained from the experiment varying ATP concentration (all other components are as noted for the standard reaction). V_{max} is reported as units per milligram GST-PKC, where one unit is defined as 1 nmol phosphate hydrolyzed per minute.

and the K_m for ATP were indistinguishable from wild-type enzyme (Fig. 2B and Table 1). However, the V_{max} was higher for PKCα-M489V [$V_{max} = (2.7 \pm 0.2) \times 10^3$ nmol phosphate per minute per mg PKC] compared with wild type [$V_{max} = (2.0 \pm 0.2) \times 10^3$ nmol phosphate per minute per mg PKC], an increase observed in each of five separate protein preparations. Analysis of protein obtained from three separate preparations, under conditions of saturating Ca^{2+} and lipid, 100 μM peptide, and 300 μM ATP, revealed a $29 \pm 9\%$ increase in the specific activity of purified PKCα-M489V compared with wild type. These data reveal that neither the degree of autoinhibition nor the cofactor-dependent release of autoinhibition is altered by the M489V mutation. Rather, Met-to-Val substitution increases the intrinsic catalytic rate of the enzyme.

Molecular Dynamics Simulations Reveal Altered Dynamics of the Catalytic Domain in PKCα-M489V. To gain insight into how the M489V mutation increases the catalytic rate without altering sensitivity to cofactors, binding of peptide substrate, or the K_m for ATP, we compared the dynamics of the kinase domain of wild type and PKCα-M489V using molecular dynamics simulations (Fig. 3). These simulations reveal both localized and long-range changes in the dynamics of the kinase core. Notably, altered dynamics were observed in two key segments of the ATP binding pocket: (i) Motion was increased in the Gly-rich loop, a key determinant between the βI and βII strands (β1/βII) that anchors the β-phosphate of ATP (33), and (ii) motion was decreased in the C-helix (αB/αC), a segment

that stabilizes the active conformation of kinases. For PKCα, Arg389 in the C-helix forms an electrostatic interaction with Glu487 in the activation loop, two residues removed from Met489, whereas the flanking Lys388 forms an H-bond with the main chain carbonyl of Gly655, part of a conserved FXXF motif (33) and two residues removed from phospho-Ser657, a key determinant of stability of PKCα's kinase domain (Fig. 1C). Additionally, the simulations indicated that motions in the distal αG and αI helices were increased in the M489V mutant compared with wild-type PKCα. These studies support a model in which replacing Met with Val at position 489 affects the dynamics not only around the active site but also at distal surfaces on the kinase domain.

PKCα-M489V Is Not More Basally Active than Wild-Type PKCα in a Cellular Environment. Given that the M489V mutation does not affect autoinhibitory constraints in the pure protein, we hypothesized that basal (unstimulated) signaling by PKCα-M489V would be similar to that of wild-type PKCα in cells. We overexpressed a FRET-based reporter for PKC activity (CKAR, ref. 34) alone or with either wild type or mutant mCherry-PKCα in COS7 cells and monitored the decrease in phosphorylation of CKAR, assessed by the decrease in FRET ratio, following addition of the general PKC inhibitor bisindolylmaleimide IV (Bis IV) (Fig. 4A). Bis IV caused a drop in the FRET ratio of cells transfected with CKAR alone, representing inhibition of the basal activity of endogenous PKC isozymes (open triangles). This
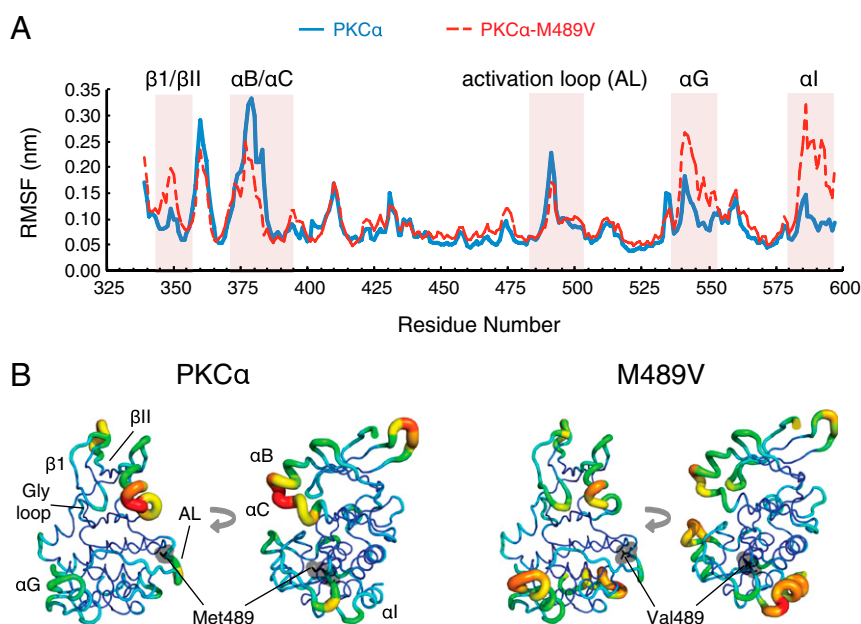

Fig. 3. M489V mutation causes key alterations in the dynamics of the kinase domain structure. (A) Molecular dynamics simulations showing altered flexibility around the ATP binding site, αG helix, and αI helix of the M489V variant. RMSF of each residue are shown (A) graphically and (B) structurally, with width and color of the ribbon corresponding to the level of fluctuations observed. Key regions are highlighted as is the residue at position 489.
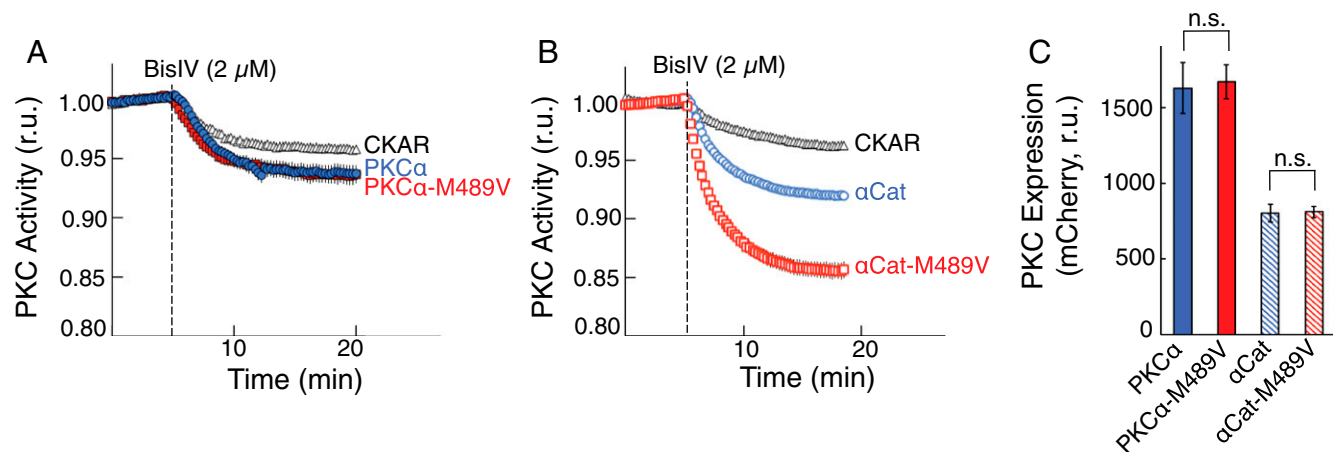
Fig. 4. Basal activity of wild type and PKCα-M489V is the same, but removal of regulatory moiety unmasks enhanced activity of the M489V kinase domain. (*A*) COS7 cells overexpressing CKAR alone (open triangles) or coexpressing CKAR and full-length mCherry-PKCα wild type (blue circles) or M489V (red squares) were exposed to 2 μM Bis IV and the change in FRET monitored ($n \geq 20$ from at least three separate biological replicates). (*B*) COS7 cells overexpressing CKAR alone (open triangles) or coexpressing CKAR and the catalytic domain of PKCα (αCat) wild type (open blue circles) or M489V (open red squares). Two micromolar Bis IV was added and the change in FRET was monitored. ($n \geq 54$ from at least three separate biological replicates). For both *A* and *B*, data were normalized to the first 5 min before Bis IV addition and are graphed as average ± SEM. Note that in some cases the error bars are obscured by the symbols. (*C*) Quantification of average mCherry-PKC expression for each overexpressed PKC depicted in *A* and *B*. Data are graphed as average mCherry intensity ± SEM (n.s., not significantly different using a Student's *t* test).

drop was larger in cells overexpressing PKCα (blue), with the difference reflecting the basal activity of the overexpressed PKCα. Importantly, Bis IV caused the same drop in cells overexpressing comparable levels of PKCα-M489V (red). Thus, the M489V mutation does not enhance the basal signaling output of PKCα; enhanced signaling is only observed following agonist stimulation and removal of autoinhibitory constraints (23).

To assess if the M489V mutation confers increased basal signaling in the absence of autoinhibitory constraints, we introduced this mutation into a PKCα construct that lacked its N-terminal regulatory moiety (thus lacking the pseudosubstrate, C1 domains, and C2 domain). We then measured the effect of inhibiting PKC activity in cells coexpressing the isolated catalytic domains (αCat) and CKAR (Fig. 4*B*). Addition of Bis IV produced a significantly higher drop in FRET for cells expressing the isolated PKCα catalytic domain containing the M489V mutation (red) compared with the wild-type PKCα catalytic domain (blue). For these experiments, cells expressing comparable amounts of each kinase domain were selected for imaging: Fig. 4*C* depicts the average mCherry-PKCα intensity for the experiments in Fig. 4 *A* and *B*. Thus, the findings in Fig. 4 *A* and *B* do not result from differences in the amount of overexpressed protein. YFP expression was used to confirm that all the experiments contained saturating levels of CKAR.

PKCα-M489V Confers Enhanced Sensitivity to ATP-Competitive Inhibitors in Cells. We next took advantage of pharmacological tools to address whether the M489V mutation alters signaling on protein scaffolds. We have previously shown that scaffold-bound PKC is refractory to ATP-competitive inhibitors such as Gö6976 and Gö6983 but is fully sensitive to the uncompetitive inhibitor Bis IV (23, 40, 41). We overexpressed both CKAR and mCherry-PKCα wild type or M489V in COS7 cells stimulated with the PKC activator phorbol 12,13-dibutyrate (PDBu) to maximally activate all PKC in the cell, followed by treatment with subthreshold amounts of the ATP-competitive inhibitor Gö6976 (Fig. 5*A*). Cells expressing PKCα-M489V displayed a greater drop in activity compared with wild-type PKCα at all three inhibitor concentrations tested. In contrast, subsaturating amounts of the ATP-uncompetitive inhibitor Bis IV caused an identical drop in the cellular activity of both wild type and PKCα-M489V (Fig. 5*B*). These results reveal that PKCα-

M489V has enhanced sensitivity to the ATP-competitive inhibitor (Gö6976) that discriminates between scaffolded and nonscaffolded PKC, but not to the nondiscriminatory inhibitor (Bis IV).

To determine whether the altered inhibitor sensitivity reflected an intrinsic property of the kinase or altered cellular interactions, we measured the K_i of purified GST-PKCα for Gö6976: The K_i of M489V (109 ± 20 nM) and wild-type enzyme (113 ± 10 nM) were the same within the error of the assay (Fig. 5*C*). These data suggest that the enhanced sensitivity of the M489V variant to Gö6976 results from altered interactions with the cellular environment, rather than from an innate property of the enzyme itself.

Phosphorylation of MARCKS Is Increased in the Brains of PKCα-M489V Mice. The M489V mutation was identified in affected, but not unaffected, siblings in four unrelated families, suggesting that it is causal in the disease (23). Because increased phosphorylation of MARCKS has been identified as one of the earliest and most robust phosphorylation changes in postmortem brains from AD patients compared with controls (28), we assessed whether the AD-associated single amino acid change altered phosphorylation of MARCKS in an animal model. To this end, we used CRISPR-Cas9–mediated genome editing to develop a genetically engineered mouse containing a homozygous M489V mutation in its *Prkca* gene (Taconic Biosciences GmbH developed for Cure Alzheimer's Fund). We obtained whole-brain lysates from either wild-type or homozygous M489V mice and analyzed them via SDS/PAGE and Western blotting for a known PKC phosphorylation site on MARCKS protein (Fig. 6). The mice containing the M489V mutation displayed a 41 ± 20% increase in phosphorylation of MARCKS at Ser-159/163 compared with wild-type mice. We also blotted for total PKCα levels to assess whether the M489V mutation affected the PKCα stability and protein levels in an endogenous, whole-brain environment. Importantly, the total PKCα protein levels were not significantly different between the wild-type and M489V samples. This establishes that the M489V mutation both changes PKCα signaling in the brain to enhance the phosphorylation of one of its major downstream targets and also does so in a manner that does not alter the steady-state levels of total PKCα protein.
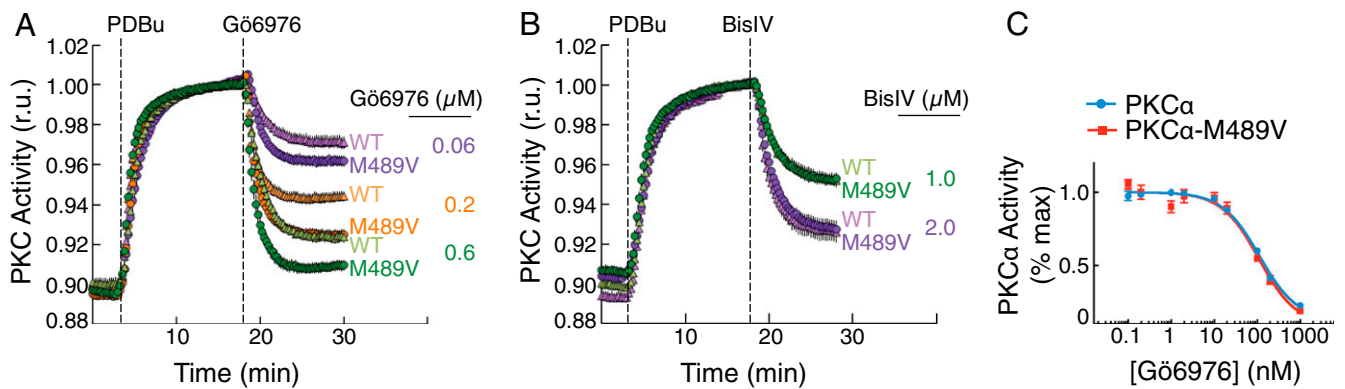
BIOCHEMISTRY

Fig. 5. PKCα-M489V in cells is more sensitive to Gö6976 inhibition. (*A* and *B*) COS7 cells overexpressing mCherry-PKCα wild type or M489V and CKAR were exposed to PDBu (200 nM) followed by subsaturating amounts of (*A*) Gö6976: 0.06 μM (purple), 0.2 μM (orange), or 0.6 μM (green) or (*B*) Bis IV: 1 μM (green) or 2 μM (purple). Data were normalized to the maximal FRET after PDBu addition. ($n \geq 14$ from three separate biological replicates). Data are depicted as average ± SEM; note that in some cases the error bars are obscured by the data points. (*C*) Purified GST-PKCα wild-type (blue) or M489V (red) activity in the presence of Gö6976. Data represent the average ± SD of triplicate samples.

Discussion

Here we unveil a previously undescribed mechanism by which a disease-associated mutation in a conventional PKC has enhanced activity without threatening the stability of the protein (Fig. 7). Biochemical and in silico approaches, cellular studies, and analysis of brains from genome-edited mice reveal that the AD-associated PKCα-M489V variant has the same on/off dynamics as wild-type enzyme but catalyzes reactions at a faster rate when on, resulting in a significant increase in phosphorylation of endogenous PKC substrates without causing a reduction in the levels of PKCα. We show that autoinhibitory constraints are unperturbed by mutation of this residue, with basal signaling both in vitro and in cells unchanged from wild-type PKCα. Rather, this mutation alters the dynamics of the kinase core in a manner that enhances the rate of catalysis by ∼30% while it is open and active, accounting for the previously described increase in agonist-evoked signaling in cells (23). Furthermore, these altered dynamics affect the cellular pharmacology of the PKCα-M489V variant, rendering it more sensitive to an ATP-competitive inhibitor but not to an uncompetitive inhibitor. Finally, we demonstrate that brains from mice with this PKCα mutation contain higher phosphorylation levels of the canonical PKC substrate MARCKS. Given this finding, it is of note that a recent unbiased phosphoproteomics study of brains from human AD patients revealed that an increase in MARCKS phosphorylation is the major up-regulated pathway in early stages of this disease (28).

The altered catalytic rate resulting from mutation of a bulky Met to the smaller Val in a key regulatory segment involved in structuring the catalytic domain's active site exemplifies how structural dynamics and protein plasticity play a critical role in catalysis. Notably, elegant NMR relaxation studies with wild-type and mutant forms of *cis–trans* isomerase cyclophilin A provide strong experimental evidence that protein motions limit the turnover rate of the enzyme (42). Consistent with protein dynamics determining the rate of catalysis, our in silico molecular dynamics simulations support a model in which substituting Met for Val at position 489 alters both localized and distal structural flexibility of the catalytic domain. Such allosteric effects are not surprising given the interlinked functional communities that populate the kinase core (33, 43). The activation loop, in particular, acts as a hub for these communities. For example, numerous studies with the archetypical kinase, PKA, and with the Tec family kinases have established that altering residues in the activation loop region alters the dynamics of the catalytic domain (44, 45). Mechanistic studies with PKA have revealed that the rate-limiting step in catalysis is the release of ADP (46). If this is

the case for PKCα, then the altered motions in the active site may reduce the constraints that limit ADP release, thereby increasing the catalytic rate. It is noteworthy that, like many enzymes (47), PKA and PKC are relatively inefficient, with PKA catalyzing on the order of 20 reactions per second (46) and PKCα on the order of 3 reactions per second (this study). Thus,
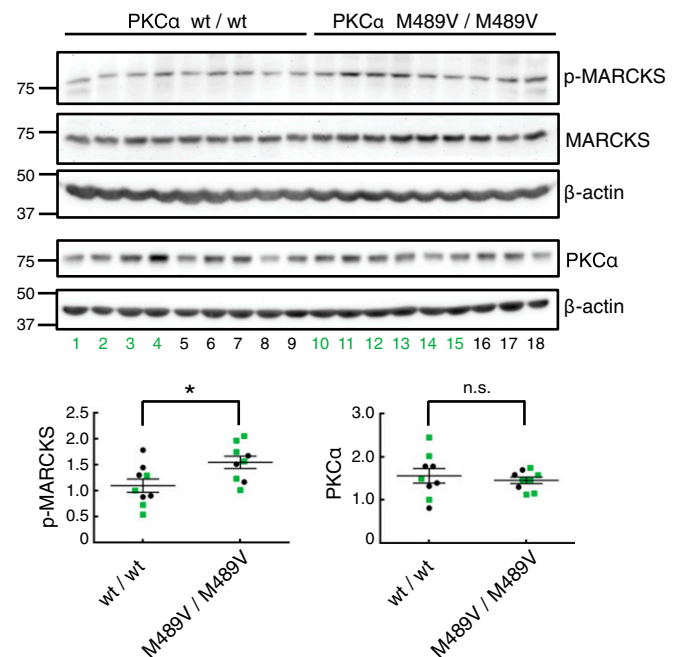

Fig. 6. Phosphorylation of MARCKS is increased in the brains of PKCα-M489V mice. Western blot of lysates of whole brain obtained from nine male and female 3-mo-old wild-type mice (lanes 1–4, males; lanes 5–9, females) or nine male and female genome-edited mice containing a homozygous PKCα-M489V mutation (lanes 10–15, males; lanes 16–18, females). Western blots were probed with antibodies specific to a known PKC phosphorylation site on MARCKS (Ser-159/163) or to total PKCα (*Top*). Bands were quantified using densitometry and the phospho-MARCKS signal was normalized to total MARCKS signal and PKCα signal was normalized to its β-actin loading control. Normalized data from the depicted Western blot were plotted (*Bottom*) as average normalized intensity ± SEM (*$P < 0.05$; n. s., not significantly different using a Student's *t* test). Males are indicated in green squares and females in black circles.
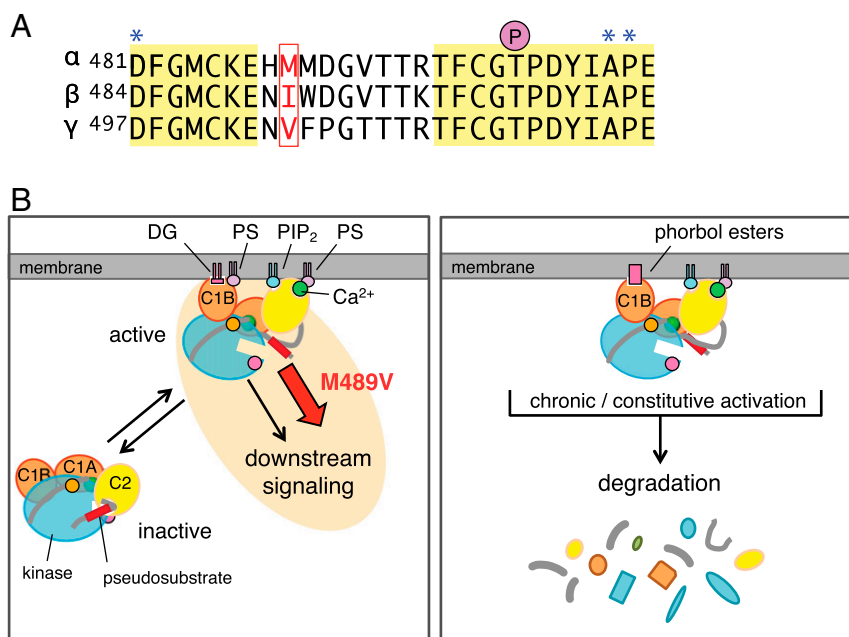
Fig. 7. PKCα-M489V mutation increases PKCα signaling output without causing PKCα degradation. (*A*) Alignment of the activation loop of conventional PKC isozymes showing conserved regions, including the flanking DFG and APE motifs, (yellow); residues that frequently harbor loss-of-function mutations in cancer (blue asterisk); and the variable residue at the position corresponding to Met489 in PKCα (red). (*B*, *Left*) Model depicting normal PKCα signaling, in which the enzyme is in an autoinhibited and stable conformation that is transiently and reversibly activated. (*B*, *Right*) Model showing the homeostatic down-regulation of PKCα after either chronic activation by phorbol esters (which trap PKC in an open and labile conformation) or as a result of mutations that disrupt autoinhibitory constraints to constitutively activate PKCα signaling. Rather than promoting the constitutively active form of PKCα that would be subsequently degraded, the PKCα-M489V mutation instead enhances the normal signaling output of the enzyme without leading to its degradation (*Left*). Domains and phosphorylation sites (small circles) are color-coded as in Fig. 1.

minor changes are likely to have significant effects on catalysis. Interestingly, the residue at position 489 varies among different PKC isozymes (Fig. 7*A*). Whether the residue at this position generally serves to tune catalytic efficiency unique to each PKC enzyme remains to be established. Indeed, there exists a precedent for residues in this position playing a key role in tuning the catalysis of kinases; namely, the large hydrophobic residue at the DFG+5 position in c-Src has been shown to act as a "hydrophobic latch" in its control of c-Src activity (48). In contrast, the flanking residues in PKC contain the highly conserved DFG and APE motifs that are frequently mutated in cancer to result in loss of function.

We have previously established that PKC bound to protein scaffolds is refractory to inhibition by ATP-competitive inhibitors (40). This is relevant to the cellular pharmacology of PKCα in the context of AD because the species of PKCα that mediates Aβ's effects on synaptic transmission depends on PKCα's PDZ ligand, which scaffolds to the PDZ domain-containing proteins PICK1 and PSD95 (25, 26). In this study, we found that PKCα-M489V gained sensitivity to the ATP-competitive inhibitor Gö6976 in cells, with sensitivity to the uncompetitive inhibitor Bis IV remaining similar to that of wild-type PKCα. In contrast, the M489V mutation did not change the IC$_{50}$ for inhibition by Gö6976 in vitro relative to wild-type protein, revealing that this altered sensitivity is specific to the cellular environment. One possible explanation is that the altered dynamics conferred by the M489V mutation now allow inhibition by ATP-competitive inhibitors, regardless of whether the kinase is bound to protein scaffolds. Alternatively, the altered dynamics may alter residency time on scaffolds. It is of note that the enhanced sensitivity of PKCα-M489V to the ATP-competitive inhibitor highlights a weakness that might be pharmacologically exploited in the treatment of this disease.

The amount of PKC activity in the cell exquisitely controls cellular homeostasis. This is exemplified by the finding that PKCβII is haploinsufficient in a colon cancer cell line: Two al-leles of this isozyme effectively suppress growth in 3D whereas one allele does not (15). Thus, small changes in the activity of PKC have large effects on cellular function. Given the multiple regulatory inputs necessary for PKC activity, PKC can be readily inactivated by mutations that prevent processing phosphorylations, impede second messenger binding, or impair catalysis. Indeed, such loss-of-function mutations are prevalent in cancer (15, 49, 50). However, mechanisms to enhance the activity of PKC are more difficult to envision. Conventional PKC isozymes engage in intramolecular autoinhibition to prevent downstream signaling in the absence of activating ligands, and disruption of this auto-inhibition by prolonged treatment with potent PKC activators such as phorbol esters and bryostatins causes the degradation of PKC (31, 32, 36) (Fig. 7*B*, *Right*). Indeed, patients receiving prolonged bryostatin infusions in a clinical trial for advanced metastatic cancer were reported to have decreased levels of PKC in peripheral blood monocytes (51). Thus, any mutations that decrease autoinhibition of PKCα to promote less constrained or constitutive activation would effectively lead to its degradation, thus par-adoxically serving as loss-of-function mutations. Here, we show that one mechanism to evade this is by increasing the reaction rate of PKC, in the absence of any perturbations of autoinhibitory constraints (Fig. 7*B*, *Left*). The ~30% increase in the reaction rate of PKCα harboring the M489V germline mutation, accumulating over a patient's lifetime, could contribute to AD pathogenesis.

The results reported here not only reveal how a subtle Met-to-Val mutation in a key region of the catalytic domain of PKCα can significantly alter molecular dynamics to increase activity—thus promoting degenerative pathology—but also highlight the importance of maintaining exactly the right level of PKC signaling, an endeavor that requires precise bio-chemical and molecular regulation.

BIOCHEMISTRY

Materials and Methods

Plasmid Constructs, Antibodies, and Reagents. The CKAR was previously described (34, 35). Human PKCα was N-terminally tagged with mCherry via Gateway cloning as described (15, 23). All mutants were generated using QuikChange site-directed mutagenesis (Agilent Genomics). The anti-PKCα antibody (610108) was from BD Transduction Laboratories. The anti-phospho PKCα/βII (pT638/641; 9375S) and pan anti-phosphorylated PKC hydrophobic motif (βII pS660, 9371S) antibodies were from Cell Signaling Technology. The pan anti-phospho-PKC activation loop antibody was previously described (52). The phospho-MARCKS (sc-12971-R) and the total MARCKS (sc-6454) antibodies were purchased from Santa Cruz Biotechnology. β-Actin antibody was purchased from Sigma-Aldrich (A2228). PDBu, Gö6976, and Bis IV were from Calbiochem. Lipids used in kinase assays (DG, 800811C and PS, 840034C) were from Avanti Polar Lipids.

Mammalian Cell Culture and Transfection. COS7 cells were maintained in DMEM (Cellgro) containing 10% FBS (Atlanta Biologicals) and 1% penicillin/streptomycin (Gibco) at 37 °C in 5% CO_2. Transient transfection was carried out using jetPRIME (PolyPlus Transfection) or FuGENE 6 transfection reagents (Roche Applied Science) for ~24 h.

PKCα-M489V Mouse Generation. C57BL/6NTac-*Prkca* mice containing the M489V mutation in *Prkca* were generated by Taconic Biosciences GmbH for Cure Alzheimer's Fund. The point mutation was inserted using a standard CRISPR/Cas9-mediated gene editing approach. In short, a ribonucleoprotein complex comprising the Cas9 protein complexed with a guide and a trans-activator crRNA molecule were injected in fertilized C57BL/6NTac oocytes along with a single-stranded oligonucleotide containing the desired point mutation. Insertion of the oligonucleotide sequence resulted in the mutation of the Met 489 to Val and introduction of an AflIII restriction site for genotyping purposes. Founder mice were genotyped by sequencing and bred to C57BL/6NTac wild-type mice for germline transmission. G1 heterozygous mice were identified by restriction analysis and confirmed by sequencing. HET G1 animals were then crossed to C57BL/6NTac wild-type mice for another generation before establishing HET × HET mating to generate cohorts for analysis. Twelve- to 15-wk old mice were used for sample preparation. All procedures involving animals were approved by The Scripps Research Institute's Institutional Animal Care and Usage Committee (IACUC) and met the guidelines of the National Institute of Health detailed in the *Guide for the Care and Use of Laboratory Animals* (53).

Murine Brain Sample Preparation and Immunoblotting. Three-month-old wild-type and homozygous M489V mice were killed and hemibrains were obtained and immediately snap-frozen. Frozen tissue was then homogenized in a dounce tissue grinder with RIPA buffer (50 mM Tris, pH 7.4, 150 mM NaCl, 2 mM EDTA, 1% Triton X-100, 1% NaDOC, 0.1% SDS, 10 mM NaF, 1 mM Na_3VO_4, 1 mM PMSF, 50 µg/mL leupeptin, 1 µM microcystin, 1 mM DTT, and 2 mM benzamidine). Homogenates were sonicated and protein was quantified using a BCA protein assay kit (Thermo Fisher Scientific). Thirty micrograms of protein were separated by standard SDS/PAGE and transferred to PVDF membranes (BioRad). Membranes were blocked with 5% BSA or 5% milk for 1 h at room temperature and analyzed by immunoblotting with specific antibodies. Detection and quantification of immunoreactive bands was conducted by chemiluminescence on a FluorChem Q imaging system (ProteinSimple). Statistical significance was determined using a Student's *t* test.

FRET Imaging and Analysis. Cells were imaged as described previously (23, 34, 54) with the following modifications: COS7 cells were cotransfected with the indicated mCherry-tagged PKC construct and CKAR (34) at a 0.8:1 ratio of DNA, respectively. Baseline images were acquired every 15 s for ≥2 min before ligand addition, and data were normalized to the baseline FRET ratios. The data are graphed as average normalized FRET ratio ± SEM from at least three independent experiments.

Insect Cell Culture and Protein Purification. Human GST-PKCα protein was expressed and purified from insect cells using the Bac-to-Bac expression system (Invitrogen). GST-PKCα protein was batch-purified using glutathione Sepharose beads as previously described (55) with the following protocol changes: Sf-21 insect cells expressing GST-tagged protein were rinsed with PBS and lysed in 50 mM Hepes, pH 7.5, 1 mM EDTA, 100 mM NaCl, 0.1% Triton X-100, 100 µM PMSF, 1 mM DTT, 2 mM benzamidine, 50 µg/mL leupeptin, and 1 µM microcystin. Purified protein was exchanged into 20 mM Hepes, pH 7.5, 1 mM EDTA, 1 mM EGTA, and 1 mM DTT using 10-kDa Amicon centrifugal filter unit (EMD Millipore). An equal volume of glycerol was then added to a final concentration of 50% glycerol for storage at −20 °C. Protein concentration was determined using (*i*) BSA standards on an SDS/PAGE gel stained with Coomassie Brilliant Blue stain and (*ii*) A_{595} of BGG standards or PKC protein after mixing 5 µL of protein solution with 45 µL of buffer (0.05 M NaOH and 20 mM Tris) and 500 µL of Coomassie (Bradford) Protein Assay Reagent (1856209; Thermo Fisher Scientific).

Kinase Assays. The activity of purified GST-PKCα (typically 2.4 nM) toward a peptide substrate (Ac-FKKSFKL-NH$_2$) was assayed as described previously (56). Standard assay conditions contained (unless otherwise specified in figure legends): Ca^{2+} (200 µM free Ca^{2+} in the presence of 500 µM EGTA), 100 µM ATP, 100 µM substrate, 5 mM $MgCl_2$, 200 µM $CaCl_2$, 0.06 mg/mL BSA, and Triton X-100 (0.1% wt/vol) mixed micelles containing 15 mol % PS and 5 mol % DG in 50 mM Hepes, pH 7.5, and 1 mM DTT. The quantities of GST-PKCα wild type or M489V used in the assay were additionally verified postassay by Western blot using a PKCα antibody. The dependence of PKC activity on Ca^{2+} or mol % PS was analyzed by a nonlinear least squares fit to a modified Hill equation as described (57) using GraphPad Prism version 6 (GraphPad Software). The K_m for peptide substrate or ATP was fit to the Michaelis–Menten equation using GraphPad Prism version 6 (GraphPad Software). The concentration of free Ca^{2+} was calculated using a program that takes into account pH, Ca^{2+}, Mg^{2+}, EGTA, and ATP concentrations (maxchelator.stanford.edu; CaMgATPEGTA program, ref. 58).

Structure Modeling and Molecular Dynamics Simulations. Homology models of PKCα wild type and M489V were created using Modeler 9.16 from Protein Data Bank (PDB) ID code 3IW4 (residues 339–597). Molecular dynamics simulations were performed using GROMACS version 5.0 with the GROMOS96 53a6 force field parameter set. All titratable amino acids were assigned their canonical state at physiological pH, short-range interactions were cut off at 1.4 nm, and long-range electrostatics were calculated using the particle mesh Ewald summation (59). Dispersion correction was applied to energy and pressure terms accounting for truncation of van der Waals forces and periodic boundary conditions were applied in all directions. Protein constructs were placed in a cubic box of 100 nM NaCl in simple point charge water with at least 1 nm distance between the protein construct and box edge in all directions. Neutralizing counterions were added and steepest decent energy minimization was performed, followed by a two-step NVT/NPT equilibration. Both equilibration steps maintained a constant number of particles and temperature, and NVT equilibration was performed for 100 ps maintaining a constant volume, followed by 10 ns of NPT equilibration maintaining a constant pressure. Temperature was maintained at 37 °C by coupling protein and nonprotein atoms to separate temperature coupling baths (60), and pressure was maintained at 1.0 bar (weak coupling). All position restraints were then removed and simulations were performed for 400 ns using the Nosé–Hoover thermostat (61) and the Parrinello–Rahman barostat (62). Root-mean-squared fluctuation (RMSF) analysis compared the SD of the atomic position of each α-carbon in the trajectory, fitting to the starting structure as a reference frame. Images were created using PyMol version 1.7.2.3.

1. Newton AC (2010) Protein kinase C: Poised to signal. *Am J Physiol Endocrinol Metab* 298:E395–E402.
2. Nishizuka Y (1995) Protein kinase C and lipid signaling for sustained cellular responses. *FASEB J* 9:484–496.
3. Pysz MA, et al. (2009) PKCalpha tumor suppression in the intestine is associated with transcriptional and translational inhibition of cyclin D1. *Exp Cell Res* 315:1415–1428.
4. Saxon ML, Zhao X, Black JD (1994) Activation of protein kinase C isozymes is associated with post-mitotic events in intestinal epithelial cells in situ. *J Cell Biol* 126:747–763.
5. Frey MR, et al. (1997) Protein kinase C isozyme-mediated cell cycle arrest involves induction of p21(waf1/cip1) and p27(kip1) and hypophosphorylation of the retinoblastoma protein in intestinal epithelial cells. *J Biol Chem* 272:9424–9435.
6. Black JD, ed (2010) *PKC and Control of the Cell Cycle* (Humana, Totowa, NJ), pp 155–188.
7. Jerome-Morais A, Rahn HR, Tibudan SS, Denning MF (2009) Role for protein kinase C-alpha in keratinocyte growth arrest. *J Invest Dermatol* 129:2365–2375.
8. Wang MT, et al. (2015) K-Ras promotes tumorigenicity through suppression of non-canonical Wnt signaling. *Cell* 163:1237–1251.

9. Newton AC, Brognard J (2017) Reversing the paradigm: Protein kinase C as a tumor suppressor. *Trends Pharmacol Sci* 38:438–447.

10. Oster H, Leitges M (2006) Protein kinase C alpha but not PKCzeta suppresses intestinal tumor formation in ApcMin/+ mice. *Cancer Res* 66:6955–6963.

11. Suga K, Sugimoto I, Ito H, Hashimoto E (1998) Down-regulation of protein kinase C-alpha detected in human colorectal cancer. *Biochem Mol Biol Int* 44:523–528.

12. Prévostel C, et al. (1995) The natural protein kinase C alpha mutant is present in human thyroid neoplasms. *Oncogene* 11:669–674.

13. Alvaro V, Prévostel C, Joubert D, Slosberg E, Weinstein BI (1997) Ectopic expression of a mutant form of PKCalpha originally found in human tumors: Aberrant subcellular translocation and effects on growth control. *Oncogene* 14:677–685.

14. Vallentin A, Lo TC, Joubert D (2001) A single point mutation in the V3 region affects protein kinase Calpha targeting and accumulation at cell-cell contacts. *Mol Cell Biol* 21:3351–3363.

15. Antal CE, et al. (2015) Cancer-associated protein kinase C mutations reveal kinase's role as tumor suppressor. *Cell* 160:489–502.

16. Bivona TG, et al. (2006) PKC regulates a farnesyl-electrostatic switch on K-Ras that promotes its association with Bcl-XL on mitochondria and induces apoptosis. *Mol Cell* 21:481–493.

17. Santiskulvong C, Rozengurt E (2007) Protein kinase Calpha mediates feedback inhibition of EGF receptor transactivation induced by Gq-coupled receptor agonists. *Cell Signal* 19:1348–1357.

18. Hunter T, Ling N, Cooper JA (1984) Protein kinase C phosphorylation of the EGF receptor at a threonine residue close to the cytoplasmic face of the plasma membrane. *Nature* 311:480–483.

19. Cochet C, Gill GN, Meisenhelder J, Cooper JA, Hunter T (1984) C-kinase phosphorylates the epidermal growth factor receptor and reduces its epidermal growth factor-stimulated tyrosine protein kinase activity. *J Biol Chem* 259:2553–2558.

20. Sipeki S, Bander E, Parker PJ, Faragó A (2006) PKCalpha reduces the lipid kinase activity of the p110alpha/p85alpha PI3K through the phosphorylation of the catalytic subunit. *Biochem Biophys Res Commun* 339:122–125.

21. Lee JY, Chiu YH, Asara J, Cantley LC (2011) Inhibition of PI3K binding to activators by serine phosphorylation of PI3K regulatory subunit p85alpha Src homology-2 domains. *Proc Natl Acad Sci USA* 108:14157–14162.

22. Hoshino D, et al. (2012) Network analysis of the focal adhesion to invadopodia transition identifies a PI3K-PKCα invasive signaling axis. *Sci Signal* 5:ra66.

23. Alfonso SI, et al. (2016) Gain-of-function mutations in protein kinase Cα (PKCα) may promote synaptic defects in Alzheimer's disease. *Sci Signal* 9:ra47.

24. Wilcox KC, Lacor PN, Pitt J, Klein WL (2011) Aβ oligomer-induced synapse degeneration in Alzheimer's disease. *Cell Mol Neurobiol* 31:939–948.

25. O'Neill AK, et al. (2011) Protein kinase Cα promotes cell migration through a PDZ-dependent interaction with its novel substrate discs large homolog 1 (DLG1). *J Biol Chem* 286:43559–43568.

26. Staudinger J, Lu J, Olson EN (1997) Specific interaction of the PDZ domain protein PICK1 with the COOH terminus of protein kinase C-alpha. *J Biol Chem* 272:32019–32024.

27. Alfonso S, et al. (2014) Synapto-depressive effects of amyloid beta require PICK1. *Eur J Neurosci* 39:1225–1233.

28. Tagawa K, et al. (2015) Comprehensive phosphoproteome analysis unravels the core signaling network that initiates the earliest synapse pathology in preclinical Alzheimer's disease brain. *Hum Mol Genet* 24:540–558.

29. Kataoka K, et al. (2015) Integrated molecular analysis of adult T cell leukemia/lymphoma. *Nat Genet* 47:1304–1315.

30. Gallegos LL, Newton AC (2008) Spatiotemporal dynamics of lipid signaling: Protein kinase C as a paradigm. *IUBMB Life* 60:782–789.

31. Kraft AS, Anderson WB, Cooper HL, Sando JJ (1982) Decrease in cytosolic calcium/phospholipid-dependent protein kinase activity following phorbol ester treatment of EL4 thymoma cells. *J Biol Chem* 257:13193–13196.

32. Szallasi Z, Smith CB, Pettit GR, Blumberg PM (1994) Differential regulation of protein kinase C isozymes by bryostatin 1 and phorbol 12-myristate 13-acetate in NIH 3T3 fibroblasts. *J Biol Chem* 269:2118–2124.

33. Kornev AP, Taylor SS (2015) Dynamics-driven allostery in protein kinases. *Trends Biochem Sci* 40:628–647.

34. Violin JD, Zhang J, Tsien RY, Newton AC (2003) A genetically encoded fluorescent reporter reveals oscillatory phosphorylation by protein kinase C. *J Cell Biol* 161:899–909.

35. Violin JD, Newton AC (2003) Pathway illuminated: Visualizing protein kinase C signaling. *IUBMB Life* 55:653–660.

36. Antal CE, Callender JA, Kornev AP, Taylor SS, Newton AC (2015) Intramolecular C2 domain-mediated autoinhibition of protein kinase C βII. *Cell Rep* 12:1252–1260.

37. Hannun YA, Loomis CR, Bell RM (1985) Activation of protein kinase C by Triton X-100 mixed micelles containing diacylglycerol and phosphatidylserine. *J Biol Chem* 260:10039–10043.

38. Orr JW, Newton AC (1992) Interaction of protein kinase C with phosphatidylserine. 1. Cooperativity in lipid binding. *Biochemistry* 31:4661–4667.

39. Orr JW, Newton AC (1992) Interaction of protein kinase C with phosphatidylserine. 2. Specificity and regulation. *Biochemistry* 31:4667–4673.

40. Hoshi N, Langeberg LK, Gould CM, Newton AC, Scott JD (2010) Interaction with AKAP79 modifies the cellular pharmacology of PKC. *Mol Cell* 37:541–550.

41. Greenwald EC, Redden JM, Dodge-Kafka KL, Saucerman JJ (2014) Scaffold state switching amplifies, accelerates, and insulates protein kinase C signaling. *J Biol Chem* 289:2353–2360.

42. Eisenmesser EZ, et al. (2005) Intrinsic dynamics of an enzyme underlies catalysis. *Nature* 438:117–121.

43. Holliday MJ, Camilloni C, Armstrong GS, Vendruscolo M, Eisenmesser EZ (2017) Networks of dynamic allostery regulate enzyme function. *Structure* 25:276–286.

44. Joseph RE, et al. (2013) Activation loop dynamics determine the different catalytic efficiencies of B cell- and T cell-specific tec kinases. *Sci Signal* 6:ra76.

45. Kornev AP, Haste NM, Taylor SS, Eyck LF (2006) Surface comparison of active and inactive protein kinases identifies a conserved activation mechanism. *Proc Natl Acad Sci USA* 103:17783–17788.

46. Zhou J, Adams JA (1997) Participation of ADP dissociation in the rate-determining step in cAMP-dependent protein kinase. *Biochemistry* 36:15733–15738.

47. Bar-Even A, et al. (2011) The moderately efficient enzyme: Evolutionary and physicochemical trends shaping enzyme parameters. *Biochemistry* 50:4402–4410.

48. Levinson NM, Seeliger MA, Cole PA, Kuriyan J (2008) Structural basis for the recognition of c-Src by its inactivator Csk. *Cell* 134:124–134.

49. Newton AC (2017) Protein kinase C as a tumor suppressor. *Semin Cancer Biol* 48:18–26.

50. McSkimming DI, et al. (2016) KinView: A visual comparative sequence analysis tool for integrated kinome research. *Mol Biosyst* 12:3651–3665.

51. Marshall JL, et al. (2002) Phase I study of prolonged infusion bryostatin-1 in patients with advanced malignancies. *Cancer Biol Ther* 1:409–416.

52. Dutil EM, Toker A, Newton AC (1998) Regulation of conventional protein kinase C isozymes by phosphoinositide-dependent kinase 1 (PDK-1). *Curr Biol* 8:1366–1375.

53. National Research Council (2011) *Guide for the Care and Use of Laboratory Animals* (National Academies Press, Washington, DC), 8th Ed.

54. Gallegos LL, Kunkel MT, Newton AC (2006) Targeting protein kinase C activity reporter to discrete intracellular regions reveals spatiotemporal differences in agonist-dependent signaling. *J Biol Chem* 281:30947–30956.

55. Tobias IS, et al. (2016) Protein kinase Cζ exhibits constitutive phosphorylation and phosphatidylinositol-3,4,5-triphosphate-independent regulation. *Biochem J* 473:509–523.

56. Keranen LM, Newton AC (1997) Ca2+ differentially regulates conventional protein kinase Cs' membrane interaction and activation. *J Biol Chem* 272:25959–25967.

57. Newton AC, Koshland DE, Jr (1989) High cooperativity, specificity, and multiplicity in the protein kinase C-lipid interaction. *J Biol Chem* 264:14909–14915.

58. Schoenmakers TJ, Visser GJ, Flik G, Theuvenet AP (1992) CHELATOR: An improved method for computing metal ion concentrations in physiological solutions. *Biotechniques* 12:870–874, 876–879.

59. Essmann U, et al. (1995) A smooth particle mesh Ewald method. *J Chem Phys* 103:8577–8593.

60. Berendsen HJC, Postma JPM, Vangunsteren WF, Dinola A, Haak JR (1984) Molecular-dynamics with coupling to an external bath. *J Chem Phys* 81:3684–3690.

61. Nose S (1984) A unified formulation of the constant temperature molecular-dynamics methods. *J Chem Phys* 81:511–519.

62. Parrinello M, Rahman A (1981) Polymorphic transitions in single-crystals–A new molecular-dynamics method. *J Appl Phys* 52:7182–7190.

BIOCHEMISTRY